The corrosion resistance of 140MXC, 530AS and 560AS coatings produced by thermal spraying

Resistencia a la corrosión de recubrimientos 140mxc, 530as y 560as producidos por proyección térmica

E. A. López Covaleda[1] and J. J. Olaya Flórez[2]

ABSTRACT

Three commercial materials were deposited using electric arc thermal spraying: 140MXC (with Fe, W, Cr, Nb), 530AS (AISI 1015 steel) and 560AS (AISI 420 steel) on AISI 4340 steel. The aim of this paper was to evaluate the best strategy for improving a coating-substrate system's corrosion resistance, using the following combinations: homogeneous single coatings, bilayers consisting of 530AS or 560AS under 140MXC and 140MXC + 530AS and 140MXC + 560AS coatings deposited simultaneously. The coatings were characterised using optical microscopy, scanning electron microscopy and X-ray diffraction. Corrosion resistance was evaluated through potentiodynamic polarisation and hardness by using the Vickers test.

Corrosion resistance depends on the amount of microstructure defects, the deposition strategy and the alloy elements. However, corrosion resistance was similar in single coatings of 140MXC and bilayers, having -630 V corrosion potential and 708 nA corrosion current. The details and corrosion mechanism of the coatings so produced are described in this paper.

Keywords: Thermal spray, corrosion, nanocomposite, multilayer, pseudoalloy.

RESUMEN

Mediante proyección térmica de arco eléctrico fueron depositados tres materiales comercialmente conocidos como: 140 MXC (a base de Fe, W, Cr, Nb), 530 AS (acero AISI 1015) y 560 AS (acero AISI 420), sobre acero AISI 4340. Con el objetivo de evaluar la mejor estrategia para incrementar la resistencia a la corrosión en el sistema capa-sustrato, los recubrimientos fueron depositados de tres formas: 1) monocapas homogéneas de cada material; 2) bicapas compuestas de una monocapa de 530 AS o de 560 AS y la segunda de140 MXC en ambos casos; y 3) recubrimientos tipo monocapa, el primero depositando de manera simultánea 140 MXC + 530 AS y otro depositando de manera simultánea 140 MXC + 560 AS. Los recubrimientos fueron caracterizados mediante microscopía óptica, microscopía electrónica de barrido y difracción de rayos X. Fue evaluada la resistencia a la corrosión por medio de polarización potenciodinámica y la dureza mediante el ensayo Vickers.

Se encontró que la resistencia a la corrosión en los recubrimientos producidos depende de la cantidad de defectos en la microestructura, de la estrategia de depósito y de los elementos en aleación. La resistencia a la corrosión fue muy similar en los recubrimientos producidos con alambres disímiles o bicapas, con un potencial de corrosión de -630 V y una densidad de corriente de 708 nm. Los detalles y mecanismos de corrosión de los recubrimientos producidos se describen en esta investigación.

Palabras clave: Proyección térmica, corrosión, nanocomposito, multicapas, pseudoaleaciones.

Received: October 11th 2011
Accepted: February 7th 2013

Introduction

Thermal spraying is becoming increasingly used in Colombia and has become the focus for research due to its easy implementation and the high quality of the coatings so produced. This process consists of projecting molten and semi-molten particles within a short time-frame onto a substrate, so that they have minimal contact with oxidising agents such as air (Deshpande, Sampath *et al*., 2006; Newbery and Grant, 2006). When these particles are deposited on a substrate or work-piece, they become deformed and compacted to produce a microstructure of rounded lamellae called "splats", which become stacked and rapidly coalesce, resulting in coating formation (Rabiei, Mumm *et al.,* 1999). These are characterised as being polycrystalline and uniform, and may be applied to improve surface properties or for recovering parts which have become worn during service. Depositing methods have become widely diversified into techniques such as flaming (characterised by high oxide content in the microstructure), arc technique (involving an intermediate quantity of defects), high velocity oxy-fuel (HVOF), and plasma (ASM 2004). The last two techniques are recognised for involving very few defects. New materials having different chemical composi-

[1] Edwin Alexis López Covaleda. Ingeniero Mecánico y Magister en Materiales y Procesos, Universidad Nacional de Colombia. E-mail: sax214@gmail.com

[2] Jhon Jairo Olaya Flórez. Magister en Materiales y Procesos de Manufactura, Universidad Nacional de Colombia. Doctor en Ingeniería, Universidad Nacional Autónoma de México. Affiliation: Profesor Asociado, Departamento de Ingeniería Mecánica y Mecatrónica, Universidad Nacional de Colombia.
E-mail: jjolayaf@unal.edu.co

How to cite: López Covaleda, E. A., Olaya Flórez, J. J., The corrosion resistance of 140MXC, 530AS and 560AS coatings produced by thermal spraying., Ingeniería e Investigación. Vol. 33, No. 1. April 2013, pp. 23-28.

tions have also been developed, such as wires, powder or powder-filled wire. The combination of techniques and materials has resulted in a wide range of industrial and research applications.

The electric arc thermal spraying technique involves using a gun having two electrically-charged wires having opposite polarity, bringing them close to each other at constant speed and creating an electric arc, which thus melts them. A stream of compressed air passes at high speed through the arc at the same time, spraying and dragging the molten material towards the substrate surface. Industry offers a wide range of products for this technique, differing in terms of coating properties, chemical composition and cost, meaning that material ranging from cheap carbon steels to complex alloys of unknown composition and high cost can be found on the market. Each wire is designed for specific applications and must be deposited with clearly defined current, potential and compressed air pressure. Different materials have been deposited and investigated in recent years; studies such as those by Edrisy, Perry *et al*.,; Edrisy, Perry *et al*., 2001, Edrisy and Alpas 2002; Jin, Xu *et al*., 2007 correlate micro-structural characterisation with wear resistance. However, little research has correlated microstructure with corrosion resistance.

On the other hand, depositing bilayers and single coatings with different materials is known in techniques such as physical vapour deposition (PVD) and chemical vapour deposition (CVD). However, this type of architecture using thermal spray processes is underdeveloped and has been under-researched. Only a few strategies are known involving the use of flame processes and powders, because it is easy to control the precursor mixture in the input hopper. A few studies have addressed such combinations of materials using an electric arc. For example, some coatings have been made using Zn, Al, and 316 to form bilayers (Lin, Lu *et al*., 2009); the production of simultaneous coatings of Al, Cu or Zn has also been explored in order to develop pseudo-alloys (mechanical mixing) and partial alloys (Syddorak, 2002). The present research was aimed at using the electric arc thermal spraying technique to obtain single coatings and bilayers using commercial products 140MXC, 560AS, and 530AS deposited on AISI 4340 steel, and furthermore to correlate corrosion resistance through potentiodynamic polarisation assays with the microstructure characterised through X-ray diffraction, hardness, optical microscopy and scanning electron microscopy (SEM).

Experimental procedure

The coatings were produced with the thermal spray technique, using the following materials: Fe-based 140 MXC tubular wire with Cr, W and Nb powder filler (Praxair Surface and Incorporated, 2006), wire having 530AS composition similar to AISI 1015 (Eutectic 2008) and 560AS wire having similar composition to AISI 410 (Eutectic 2007). These materials were deposited using three strategies or architectures, as seen in Figure 1: three independent monolayers composed of 140MXC, 530AS, and 560AS, two bilayers composed at the bottom of 560AS or 530AS and at the second layer of 140MXC in both cases and two coatings deposited simultaneously using dissimilar wires 530AS + 140MXC in the first case and 560AS + 140MXC in the second case. All coatings were deposited on AISI 4340 steel (ASM, 1990) substrates having ~5 GPa hardness, polished with an abrasive disc to 0.5 roughness (Ra) and also cleaned with acetone and isopropanol in ultrasonic immersion. The substrates were blasted with 96.04% purity aluminium oxide using 413X103 Pa pressure, according to published recommendations (Mellali, Grimaud *et al*., 1997; Wang, Li *et al*., 2005; Patel, Doyle *et al*., 2010), consuming up to 3.108 cm^3/cm^2 on average to get white metal having 2.2 roughness (Ra).

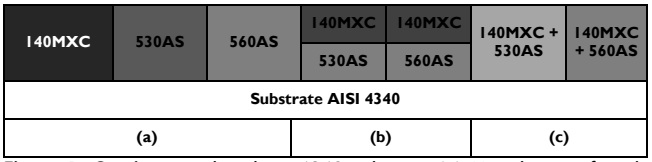

Figure 1. Coatings produced on 4340 substrate (a) Monolayers of each material, (b) bilayers of 530AS with 140MXC and 560AS with 140MXC, and (c) monolayers 530AS+140MXC and 560S + 40MXC

The Eutronic Arc Spray 4 system was used to produce the coatings in this investigation, using the parameters shown in Table 1; these parameters were established after studying the range recommended by the manufacturer for each material.

Table 1. Deposition parameters for the coatings so produced

Deposit parameter	Value	Unit
Chamber pressure	$4X10^6$	Pa
Pressure in the "arc jet"	$4X10^6$	Pa
Amperage	130-150	A
Voltage	30-35	V
Projection distance	0.33	M

Corrosion resistance was evaluated through potentiodynamic polarisation tests using Gamry 600 equipment, following ASTM G3 and G5 (ASTM 2010) recommendations. High purity graphite was used as a counter electrode and a saturated calomel electrode (SCE) as reference electrode in the tests. A 3% NaCl solution was used as an electrolyte, with -0.3 V initial potential, 0.4 V final potential, 6.030 pH at room temperature, -0.3 V initial potential, 0.4 V final potential, 0.5 mV/s scan rate and 0.196 cm2 exposed area. A 45-minute solution settling time after sample immersion was allowed for all tests.

The structural study involved X-ray diffraction (XRD) using an X-Pert Pro analytical system for grazing incidence and Bragg-Brentano configurations and monochromatised CuK α radiation (1.540998 A) functioning at 45 kV and 40 mA. Morphology was determined with a scanning electron microscope (FEI QUANTA 200 SEM) using high vacuum and 30 KV voltage. Hardness was measured with a Vickers micro-hardness tester using a Leco, with a 300g load for 15 sec.

Results and Discussion

Figure 2 shows the XRD spectra for the coatings produced in this investigation. The 140MXC coating had one signal which may have been FCC, or simple HCP iron, or Fe alloyed with Cr, Nb, or W. This was likely due to the formation of an amorphous structure, which may have had its origin in the size of the filler powders in 140MXC tubular wire. Previous research (Castellanos Dimate LM, 2011) using transmission electron microscopy (not shown) identified the formation of randomly orientated nanograins in an amorphous matrix. The same pattern was seen in the 140MXC + 560AS and 140MXC + 530AS bilayers, possibly being associated with 140MXC layer thickness, which was greater than 50μm, and this may have impeded X-ray beam penetration through the lower coating.

The BCC structure of alpha iron with mixed orientation planes (110), (200), (220), (310) and (310) was found in the 530AS and 140MXC + 530 AS coatings. It was also observed that the 140MXC +530 AS sample had less signal intensity, close to 45°, which may have been attributed to the formation of an amorphous structure. The XRD pattern found in the 530AS coating

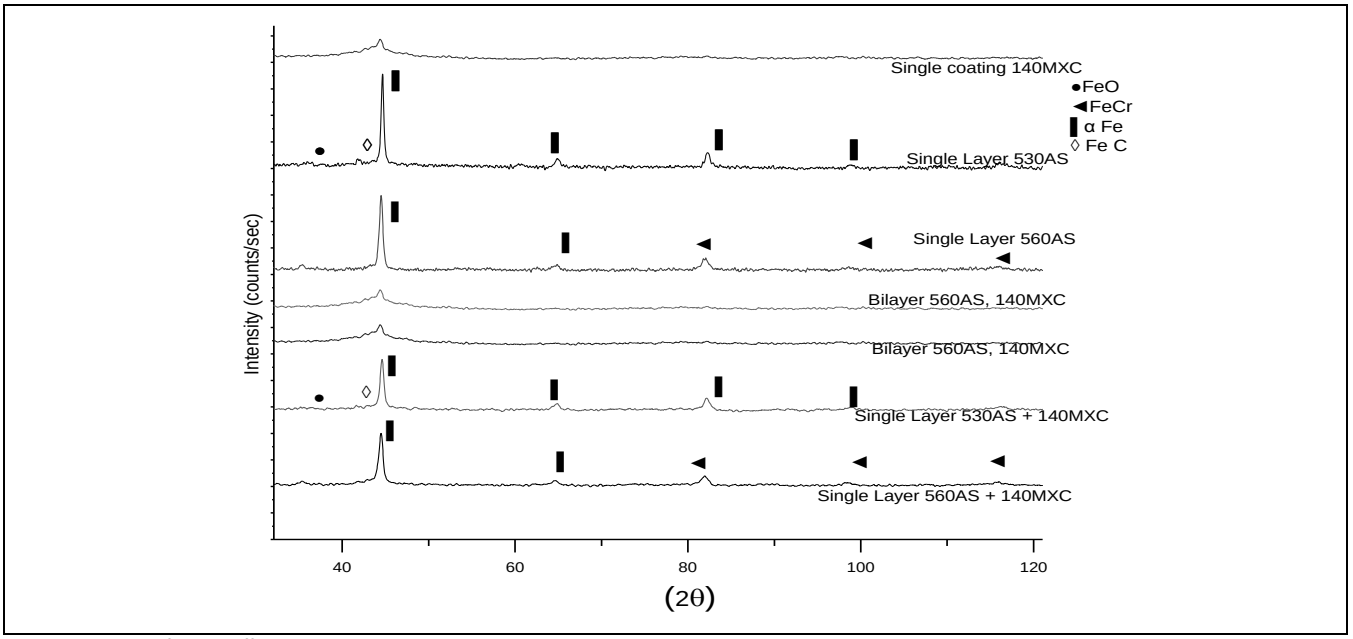

Figure 2 Patterns of X-ray diffraction carried out on the coatings so produced

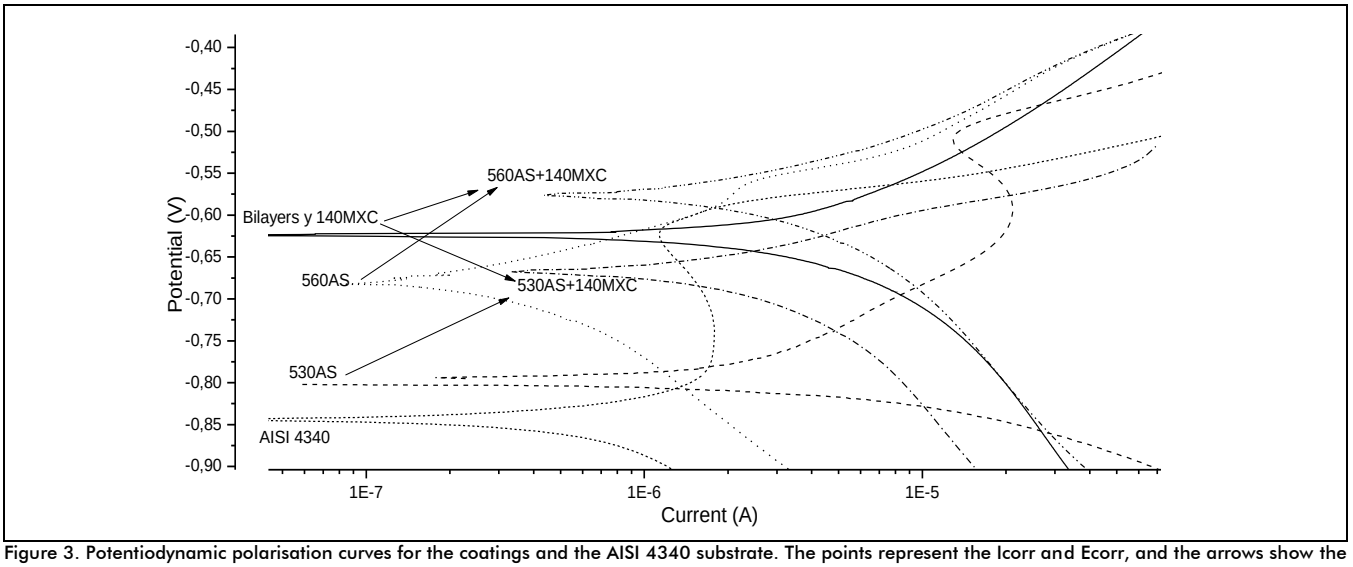

Figure 3. Potentiodynamic polarisation curves for the coatings and the AISI 4340 substrate. The points represent the Icorr and Ecorr, and the arrows show the change in the materials' properties when they were deposited simultaneously.

was consistent with other studies using the same steel deposited using an electric arc (Edrisy, Perry *et al*., 2001). Furthermore, the 560AS sample showed the BCC alpha iron structure with chromium as a solution with compositions (CrFe4 Cr1.07Fe18.93 Cr0.03Fe0.97 Cr1.36Fe0.52) randomly distributed in planes (110) (200) (211) (220), thereby agreeing with other studies (Jin, Xu *et al*. 2007). These signals' intensity decreased when 140 MXC wire was added to the coating, due to amorphous formation.

Figure 3 shows the coatings' potentiodynamic polarisation curves and those for the substrate. This illustrates the points corresponding to the calculated potential and corrosion current for each curve. The polarisation curves overlapped for the MXC 140 sample and the bilayers, which may have indicated that the electrolyte only interacted chemically with the surface of the coating, with little diffusion through its thickness. It can also be observed that the 560AS and 530AS coatings increased the corrosion current when they were simultaneously deposited with the 140MXC wire. However, the effect was the opposite in the latter material; this was possibly due to the formation of a passivation layer consisting of Cr and Nb oxides, (Valencia, 1986) (Cheng, Bullerwell *et al*., 2003) which allowed the corrosion current to become reduced. The curves obtained confirmed the increase in 560AS + 140 MXC and 560AS +140 MXC monolayer corrosion potential regarding the precursor materials. Table 2 gives a summary of the results for the current (Icorr) and the corrosion potential (Ecorr), calculated from the potentiodynamic polarisation curves. These results showed that corrosion resistance did not change significantly when the 140 MXC wire was combined with steel wires.

All the coatings produced were observed in cross-section using optical microscopy, and the structures were defined depending on the etchant. Figure 4 shows monolayers and bilayers attacked by Nital and Vilella. Nital allows the carbon steel structure to be appreciated (see mark 2 in b and d) and Vilella facilitates observation of steel having high chromium content (see mark 3 in CYE),

thereby facilitating differentiating the splats produced by wires used as precursors (ASTM 2007).

Table 2. Summary of results of Icorr and Ecorr, calculated from potentiodynamic polarisation curves

Sample	Icorr (A)	Ecorr (V)
530AS 140MXC bilayer	6.85X10E-6	-646.7
560AS 140 MXC bilayer	7.24X10E-6	-611.5
140MXC monolayer	7.17X10E-6	-632.5
530AS monolayer	3.10 X10E-	-799
560AS monolayer	0.45 X10E-	-682.25
530AS + 140MXC monolayer	4.9 X10E-6	-657.4
560AS + 140MXC monolayer	3.50 X10E-	-576
AISI 4340 substrate	0.59 X10E-	-833.33

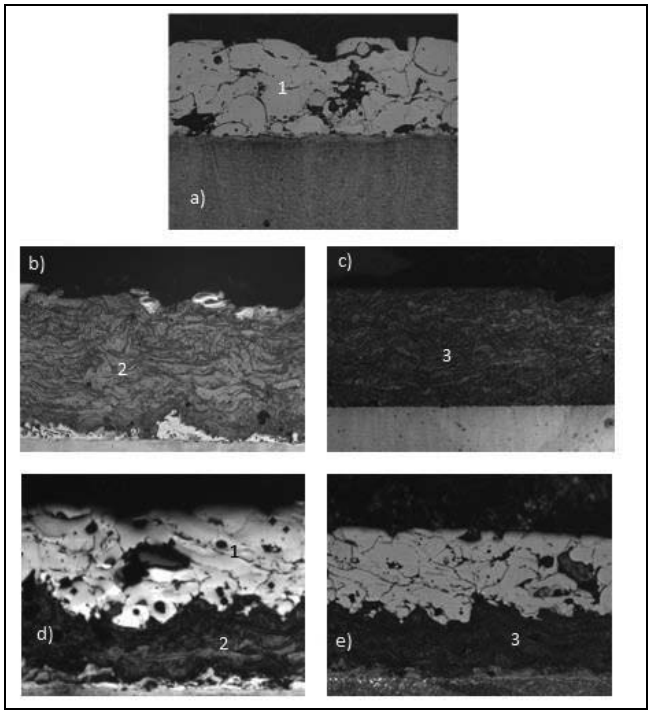

Figure 4. Optical images in cross-section at 50X a) 140MXC monolayer b) 530AS monolayer, c) 560AS monolayer d), 530AS/140MXC bilayer and e) 460AS/140MXC bilayer

The reactive used did not attack the 140MXC coating. Figure 5 shows a cross-section using optical microscopy on monolayers deposited with dissimilar wires; 530AS +140 MXC was etched with Nital and 560AS +140 MXC 560AS with Vilella. The white shown in these results represents 140MXC splats, the gray tones were mixed, and the dark colours were 530AS and 560AS splats; un-melted particles were also observed as round elements.

Table 3. Chemical composition, reference values and average of monolayer coatings taken through EDX. The measurements were taken regarding the numbered areas shown in Figures 4 and 5

Measurement zone	Material	Alloy %							
		Fe	C	Cr	Mn	W	Mo	Nb	Al
1	140MXC	57.8	3.3	15.9		9.7	2.3	5.4	4.2
2	530AS	84.6	0.18		0.7				
3	560AS	80.4		15.2					
4	530AS +140MXC	54.1	3.4	15.3		15.3	2.3	3.8	1.1
5	530AS +140MXC	86.0	0.14		0.7				
6	560AS +140MXC	81.8		14.8					

Table 3 gives the average values for chemical composition through EDX, and Table 4 shows hardness, taken from the substrate/coating interface towards the coating surface. The areas numbered on the microstructures presented in Figures 4 and 5 were thus considered. It can be seen that neither the chemical composition nor hardness changed significantly in the coating with the two strategies used; also, the partial mixtures had their precursors' average values, possibly because of the elemental diffusion caused by the concentration difference as a driving force. Furthermore, 140 MXC coating hardness values decreased considerably when it was combined with carbon or stainless steel wires. This suggested that these mixtures could reduce the system's wear resistance.

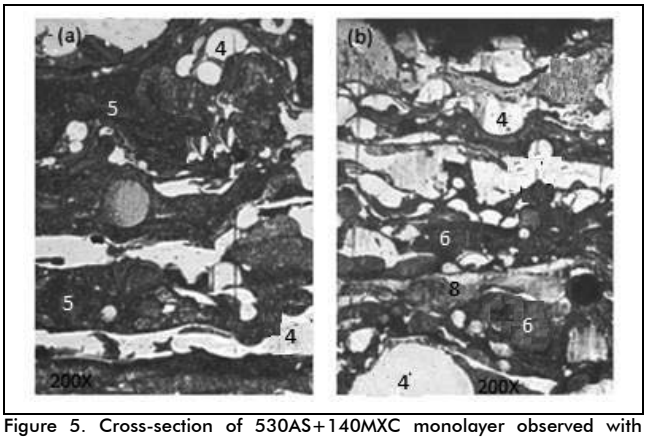

Figure 5. Cross-section of 530AS+140MXC monolayer observed with optical microscopy at 200X (a) attacked by Vilella and 560AS+140MXC (b) attacked by Pical

Table 4. Average hardness taken from the substrate to the surface

Material	Hardness (GPa) Substrate → Coating surface				
140MXC	10.3	9.4	9.6	10.1	9.4
530AS	2.4	3.1	2.5	3.4	3.1
560AS	4.4	3.9	4.1	3.2	3.7
530AS+140MXC	9.3	10.2	9.7	9.5	10.0
530AS+140MXC	3.2	3.3	2.4	3.3	2.6
560AS+140MXC	3.8	4.2	4.3	3.3	3.7

The specimens were cut in cross-section after the corrosion test to observe coating diffusion on the substrate. Figure 6 shows the SEM cross-section of a) bilayer 140MXC/530AS, b) 530AS coating and c) 560AS coating. The coating was observed to be without degradation, corrosion residues, layer detachment or adhesion loss in all three cases. These results could have been attributed to the electrolyte only interacting chemically with the surface and low diffusion for electrolyte grain boundaries, cracks and gaps.

Figure 7 shows 530AS +140 MXC and 560AS + 140MXC coatings' surface and cross-section. Corrosion and corrosion paths through splat boundaries can be observed, such defects allowing galvanic coupling. These coatings' corrosion mechanism was related to defects such as porosity, un-melted and/or semi-molten particles, oxides, and micro-cracks, which allowed the electrolyte to penetrate from the coating surface towards

the substrate surface. It could thus be established that a great many anions, Cl ions, promoted substrate reaction with the 3% NaCl solution. An anodic reaction on the coating surface and a cathodic reaction in the vicinity would thus be generated.

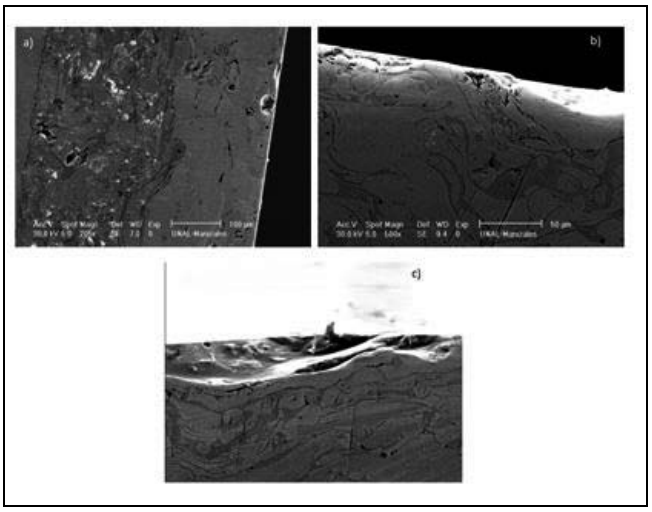

Figure 6. SEM cross-section after the corrosion test following electrochemical corrosion a) and b) bilayers 140MXC+530AS, c) monolayer 530AS, and d) monolayer 560AS

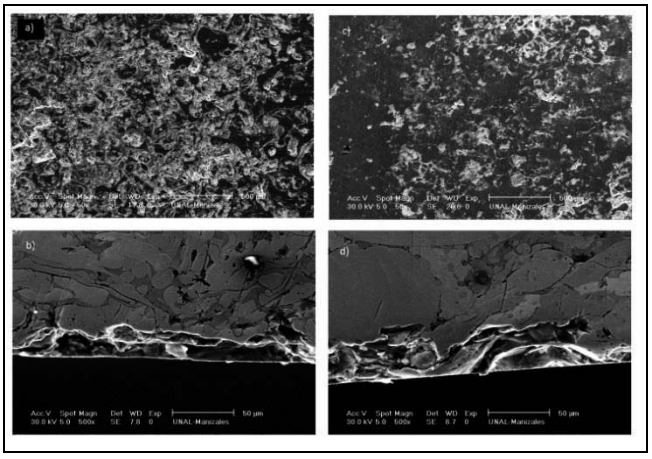

Figure 7. SEM 500X image of coating surface and cross-section a) and b) 530AS + 140MXC, c) and d) 560AS + 140MXC coatings after the corrosion test

Conclusions

140MXC (based on Fe, W, Cr, Nb), 530AS (AISI 1015) and 560AS coatings (AISI 420) were deposited on AISI 4340 steel using the electric arc thermal spray technique and the same deposition parameters and were evaluated for corrosion resistance.

The 140MXC monolayer and bilayers proved to have very similar polarisation curves, thus indicating that the electrolyte mainly interacted with the top bilayer. This suggested that combining 140MXC wire with carbon or stainless steel wire would not lead to a reduction in an industrial application's corrosion resistance.

Moreover, the simultaneous monolayer's polarisation curve differed from its precursors and did not agree with the mixed potential theory; further investigation of corrosive phenomena is thus needed, using another technique, for instance electrochemical impedance spectroscopy.

Hardness became considerably reduced in the coating obtained with dissimilar wires or using bilayers. Perhaps this would be a disadvantage when applied to surfaces subject to wear or when subjected to high loads.

Pseudo alloys or mechanical mixtures from their wire precursors were formed when coatings were produced with dissimilar wires, possibly due to the high cooling rates and multiplicity of nucleation sites. Furthermore, since defects such as cracks, voids, oxides and un-melted particles were present in coatings having 140MXC wire, it is recommended that an optimisation study should be carried out regarding deposition to improve final coating quality and density.

Acknowledgements

The financial support for this research was given by el Patrimonio Autónomo Fondo Nacional de Financiamiento para la Ciencia, la Tecnología y la Innovación, Francisco José de Caldas.

References

ASM (1990). Properties and selection: irons, Steels, and hi performance Alloys, ASM.

ASM (2004). Handbook of thermal spray technology. USA, ASM International.

Astm (2007). Standard practice for microetching Metals and Alloys. E407: 23.

Astm. (2010). "G3-89(2010) Standard Practice for Conventions Applicable to Electrochemical Measurements in Corrosion Testing." from:

http://www.bases.unal.edu.co:4323/SUBSCRIPTION/filtrexx40.cgi?+/usr6/htdocs/newpilot.com/SUBSCRIPTION/REDLINE_PAGES/G3.htm.

Cheng, Y. F., J. Bullerwell, et al. (2003). "Electrochemical investigation of the corrosion behavior of chromium-modified carbon steels in water." Electrochimica Acta 48(11): 1521-1530.

Deshpande, S., S. Sampath, et al. (2006). "Mechanisms of oxidation and its role in microstructural evolution of metallic thermal spray coatings--Case study for Ni-Al." Surface and Coatings Technology 200(18-19): 5395-5406.

Edrisy, A. and A. T. Alpas (2002). "Microstructures and sliding wear resistances of 0.2% carbon steel coatings deposited by HVOF and PTWA thermal spray processes." Thin Solid Films 420-421: 338-344.

Edrisy, A., T. Perry, et al. "The effect of humidity on the sliding wear of plasma transfer wire arc thermal sprayed low carbon steel coatings." Surface and Coatings Technology 146-147: 571-577.

Edrisy, A., T. Perry, et al. (2001). "Wear of thermal spray deposited low carbon steel coatings on aluminum alloys." Wear 251(1-12): 1023-1033.

Eutectic, C. (2007). Techinical data ARC 560 Wire.

Eutectic, C. (2008). Technical data ARC 530 wire.

Jin, G., B.-s. Xu, et al. (2007). "Microstructure and tribological properties of stainless steel coatings sprayed by two methods based on spraying." Surface and Coatings Technology 201(9-11): 5261-5263.

L.M. Dimaté Castellanos, J. J. O. F., E.A. López Covaleda, J.A. Morales Torres (2011). "Producción y resistencia a la corrosión de recubrimientos de WC-Co y Fe-Nb-Cr-W aplicado por la técnica de proyección térmica para aplicaciones en la industria naval." Escuela Colombiana de Ingeniería.

Lin, B.-l., X.-y. Lu, et al. (2009). "Corrosion behaviors of arc spraying single and double layer coatings in simulated Dagang soil solution." Transactions of Nonferrous Metals Society of China 19(6): 1556-1561.

Mellali, M., A. Grimaud, et al. (1997). "Alumina grit blasting parameters for surface preparation in the plasma spraying operation." Journal of Thermal Spray Technology 6(2): 217-227.

Newbery, A. P. and P. S. Grant (2006). "Oxidation during electric arc spray forming of steel." Journal of Materials Processing Technology 178(1-3): 259-269.

Patel, K., C. S. Doyle, et al. (2010). "Effect of surface roughness parameters on thermally sprayed PEEK coatings." Surface and Coatings Technology 204(21-22): 3567-3572.

Praxair Surface, t. and T. Incorporated (2006). Praxair and Tafa

140 MXC tm Nano compisite Wire.

Rabiei, A., D. R. Mumm, et al. (1999). "Microstructure, deformation and cracking characteristics of thermal spray ferrous coatings." Materials Science and Engineering: A 269(1-2): 152-165.

Syddorak, V. M. P. V. M. D. I. I. (2002). "Cu-Al and Zn-al antifriction electric-arc coatings." Materials science 38: 3.

Valencia, A. (1986). Tecnologia del tratamiento termico de los metales. Medellin, Universidad de Antioquia.

Wang, Y. Y., C. J. Li, et al. (2005). "Influence of substrate roughness on the bonding mechanisms of high velocity oxy-fuel sprayed coatings." Thin Solid Films 485(1-2): 141-147.